Journal of Geointerface, Vol. 5, No. 2, December 2026, pp. 1–17 e-ISSN: 2583-6900

Significance of Grain-Size Reduction and Clast Frequency–Size Variations in the Salem Pseudotachylites, south India

Honey H. Das [1,*], A. Bhattacharya [2], Antony Gilroy [1], Naveen P.U. [1]

[1] *Department of Marine Geology and Geophysics, School of Marine Sciences, Cochin University of Science and Technology, Kochi 682 016, India*
[2] *180B, Hijli Co-operative Society, Kharagpur 721 306, India*

ABSTRACT
Size-frequency analyses of monomineralic and polymineralic clasts (host-rock fragments) with equivalent radii of 20–950 µm were conducted on three centimetre- to sub-centimetre-wide pseudotachylite veins hosted by charnockite mylonites from Salem, South India, to determine whether the fine-grained matrix consists predominantly of quenched melt and micro-phenocrysts or aggregates of ultra-fine host-rock fragments. The grain size distributions (GSDs) of monomineralic and polymineralic clasts are distinct and do not conform to the commonly assumed fractal power-law relationship ($N = C/r^D$, where N is the number of clasts of radius r, C is a proportionality constant, and D is the fractal dimension, $2 < D < 3$). Instead, the GSDs are better described by truncated Gaussian distributions, with truncation in the finer size range resulting from limited resolution of size-frequency data. Although the GSDs can be approximated by a power-law relationship when larger bin sizes are used, this approximation is restricted to the analysed size range, is non-fractal, and lacks genetic significance. The cumulative area of clasts finer than the analysed size range is estimated to constitute only a small proportion of the non-clast fine-grained matrix, which accounts for approximately 75–80% of the vein area. Consequently, the matrix in the Salem pseudotachylites is interpreted to consist predominantly of quenched frictional melt and micro-phenocrysts crystallized from the melt, rather than aggregates of ultra-fine host-rock fragments.

ARTICLE HISTORY
Received: 03 July 2026
Revised: 20 Aug 2026
Accepted: 23 Aug 2026

https://doi.org/10.5281/zenodo.22088771

KEYWORDS
Pseudotachylite
clast
size-frequency distribution
Gaussian distribution
power law distribution
frictional melt

1. Introduction

Field studies (Brown and Solar, 1998; Hand and Dirks, 1992; Rosenberg, 2001; Bhadra et al., 2007) and experimental investigations (Caricchi et al., 2007; Champallier et al., 2008) suggest that the presence of melt decreases the viscosity of partially molten rocks, thereby promoting the localization of deformation strain in actively deforming crust (Petford et al., 1993; Vigneresse et al., 1996). In addition, friction-induced melts may lubricate fault zones and profoundly influence fault movement and palaeoseismic processes. Therefore, understanding the origin and nature of friction-induced melts is fundamental to interpreting the mechanics of seismic faulting.

One important manifestation of friction-induced melting is pseudotachylite, which commonly occurs as intrusive veins and sheets within fault zones (Shand, 1916). The origin of its ultra-fine-grained, dark-colored matrix has been the subject of recurrent debate. Two major interpretations continue to be discussed: does the ultra-fine-grained matrix represent quenched silicate melt produced by frictional melting in fault zones (Macaudiere et al., 1985; Toyoshima, 1989; Skrotzki et al., 1990; Obata and Karato, 1995; Gibson, 2002; Plattner et al., 2003; Lund and Austrheim, 2003; Hirose and Shimamoto, 2005; Han et al., 2007; Clarke and Norman, 2007; Lieger et al., 2009; Patro et al., 2011), or does the dark aphanitic

*Corresponding author. Email: honeyhdas@cusat.ac.in, honeysouparnika@gmail.com (HHD), abbhat55@gmail.com (AB), antonygillroy@gmail.com (AG), punaveenpu@gmail.com (NPU)

matrix comprise aggregates of mechanically crushed, ultra-fine clasts derived from the comminution of minerals and host rocks (Wenk, 1978; Wenk et al., 2000; Janssen et al., 2010).

Distinguishing between these two interpretations is challenging because the size and abundance of the finest clasts, which constitute a substantial proportion of the aphanitic matrix, are difficult to measure directly. These parameters may therefore be assessed by extrapolating the size–frequency distribution of measurable larger grains to the finest size fraction. A sharp reduction in the frequency of finer-sized clasts may indicate that the bulk of the aphanitic matrix is glassy and represents friction-induced melt. In contrast, if the frequency of clasts increases with decreasing clast size within the observable size range, the aphanitic matrix is likely to be dominated by aggregates of comminuted host-rock grains.

Consequently, grain-size distributions have been widely used to investigate the origin of pseudotachylite matrices. Several studies (Mandelbrot, 1982; Sammis et al., 1987; Okamoto and Kitamura, 1990; Shimamoto and Nagahama, 1992; Blanpied et al., 1995; Ray, 1999; Chester et al., 2005; Wilson et al., 2005; Keulen et al., 2007), grain size distribution of clasts in pseudotachylite has been approximated by the power law relation, e.g. $N_n = C/{r_n}^D$ (N_n and r_n are number and length respectively in n clasts; C is the proportionality constant, and D is the power law exponent, termed the fractal dimension; Turcotte, 1992). The log-linear expression for the power law function is

$$\log(N_n) = \log(C) - D.\log(r_n).$$

In log (N_n) versus log (r_n) plots, the abundance of the finer-sized clasts in pseudotachylite and fault gauge increase linearly with decreasing grain size. However, well-correlated straight-line fit to the entire size-frequency range of clasts in pseudotachylites is barely reported, and instead, the finer-sized grains are commonly observed to "fall off" the linear trend, i.e. the measured abundances of the finer sizes are lower in abundance relative to that predicted by the straight line fit based on the size-frequency variations in the coarser size fractions (Shimamoto and Nagahama, 1992; Ray, 1999).

Several mechanisms have been proposed to explain this deviation from the ideal power-law behavior. Ray (1999) suggested that the "fall-off" in the finer size range was caused by neglecting melt layers of uniform thickness surrounding the comminuted clasts following melting. To accommodate the increase in effective radius in clasts due to the melt layers of uniform width, Ray (1999) adopted the modified form of the power law equation, e.g. $N = N' (1 + d/d')^{-D}$ (with N' and d' as additional constants) proposed by Shimamoto and Nagahama (1992) to explain grain size distributions (GSDs) in pseudotachylites. However the "fall-off" in the finer size range is also evident in fault gouges in granitoids (Keulen et al., 2007) in which friction-induced melts are demonstrably absent. Therefore, the "fall-off" in the finer-size range may not be genetically linked to the melt films.

Alternatively, comminution may produce grain-size distributions that do not conform to a power-law relationship. For example, synthetically crushed rocks are known to exhibit normal grain-size distributions (Raisanen et al., 2006). Furthermore, size reduction of clasts may not follow a uniform geometric pattern because the comminution of mineral and rock fragments can be influenced by their rheological characteristics (Mogi, 1974; Davidage, 1979; Blenkinsop and Sibson, 1992; Tromans and Meech, 2002; Spray, 2010) and by the dominant size-reduction processes, including rupturing, wear, and attrition (Keulen et al., 2007; Pec et al., 2012). These observations indicate that the origin of the observed grain-size distributions remains unresolved and that the assumption of universal fractal behavior requires further evaluation.

In this study, we present the results of grain-size distribution (GSD) analysis of pseudotachylite veins hosted by charnockitic mylonites from Salem, South India. We demonstrate that the GSDs of the Salem pseudotachylite veins do not increase asymptotically with decreasing grain size, as predicted by the power-law approximation. Instead, the frequency of clasts initially increases and subsequently decreases with decreasing grain size. The "fall-off" of finer-sized clasts from the log–log linear fits to the power-law relationship is consistent with observations reported in earlier studies. However, the "fall-off" is minimized and the GSDs are linearized by appropriately stretching the class intervals of clast size. We further attempt to explain the "fall-off" in the non-fractal GSDs as a consequence of grain-size reduction coupled with melting.

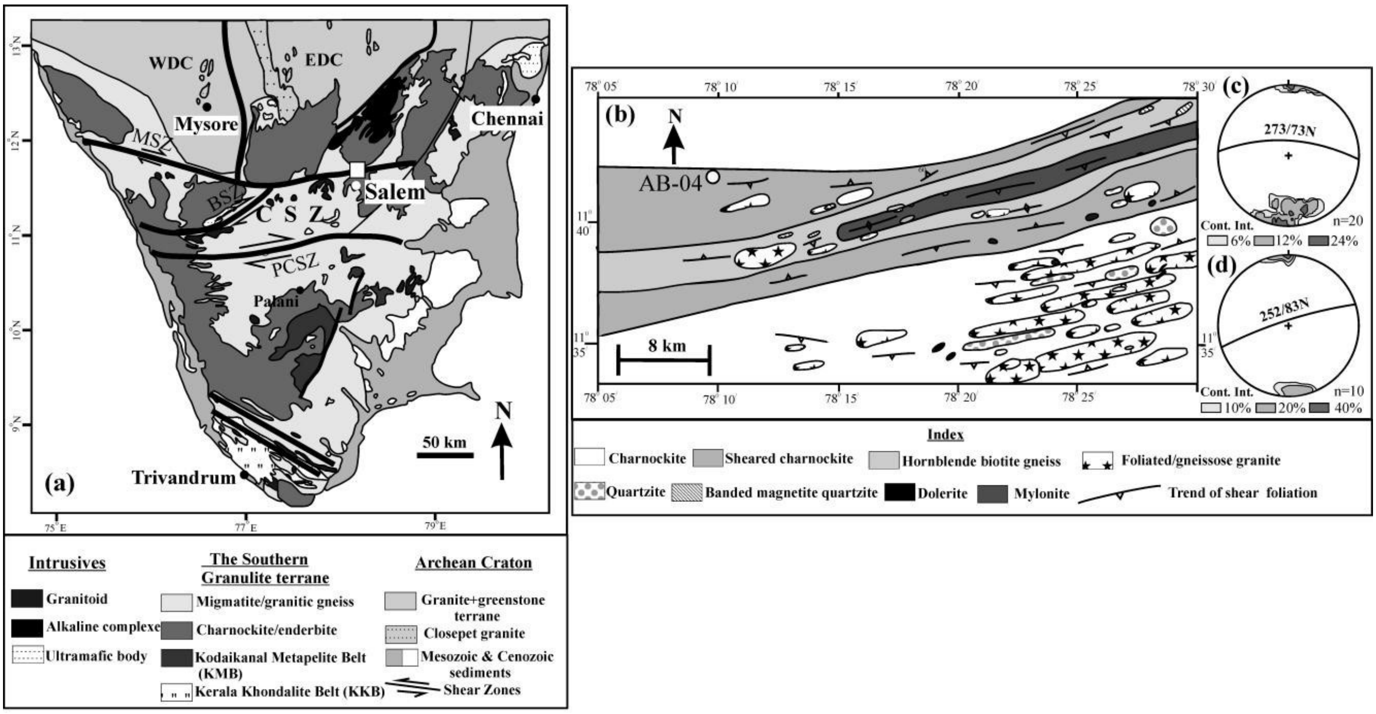

Fig. 1. (a) Map of South India showing the Southern Granulite Terrain dissected by the Paleozoic /Neoproterozoic shear zones of the Palghat–Cauvery Shear Zone system. The location of Salem (in the Salem–Attur shear zone, SASZ) is indicated. Abbreviations – WDC: western Dharwar craton, EDC: eastern Dharwar craton, MSZ: Moyer shear zone, BSZ: Bhavani shear zone, (b) Geological map of the study area, modified after Satheesh Kumar and Prasannakumar (2009). The analyzed sample AB04A-J & I is located in the figure. (c, d) Great circles in stereogram shows the mean orientations of the (c) early gneissic foliation in charnockites and the (d) shear zone foliation, corresponding to the maxima of the measured poles (contoured).

2. Geological background

A network of anastomosing Early Paleozoic to Late Neoproterozoic shear zones dissects the Southern Granulite Terrain, SGT into several Mesoarchean through Neoarchean to Paleoproteroizc domains (Fig. 1a). The shear zones in the Palghat–Cauvery shear system (PCSS, Drury and Holt, 1980) are polychronous, e.g. the Moyar Shear Zone (MSZ - Sm-Nd garnet: 624-591 Ma, Rb-Sr biotite: 604–540 Ma), the Bhavani Shear Zone (BSZ - Sm-Nd garnet: 522 Ma, Rb-Sr biotite: 521–491 Ma) and the Cauvery Shear Zone (CSZ - Sm-Nd garnet: 521 Ma, Rb-Sr biotite: 488–485 Ma) (Raith et al., 1999; Bhaskar Rao et al., 1996, 2003; Meißer et al., 2002; Brandt et al., 2011).

The present study area is located near the Sellnaicekenpally bypass (11°37.32′N, 78°09.083′E), close to Salem, Tamil Nadu (Fig. 2b), within the Salem–Attur Shear Zone (SASZ). The SASZ is widely regarded as the eastern continuation of the Moyar Shear Zone (MSZ), representing one of the major crustal-scale shear systems in the Southern Granulite Terrane (Drury et al., 1984; Chetty, 1996; Raith et al., 1999; Bhadra, 2001; Ramakrishnan, 2003; Jain et al., 2003). The shear zone is dominated by charnockite gneisses containing enclaves of mafic granulites, banded magnetite quartzite, and hornblende-biotite gneiss. These lithologies are intensely deformed within the ENE-trending dextral shear zone (Biswal et al., 2010). In high-strain domains, the original gneissic foliation (Sg) is progressively rotated and transposed into parallelism with the mylonitic foliation (Sm), reflecting intense ductile deformation (Fig. 2a, b).

Pseudotachylite veins are predominantly restricted to the mylonitic domains and display a wide variety of geometric patterns (Fig. 2). The thicker veins generally occur parallel to the mylonitic foliation (Sm), indicating strong structural control by the shear fabric (Fig. 2a, b). In contrast, thinner (typically a few millimetres thick) and shorter injection veins are preferentially aligned sub-parallel to the C and C′ shear bands as well as the host gneissic foliation (Sg) within the charnockites (Fig. 2b). In relatively low-strain domains, pseudotachylites form anastomosing vein networks enclosing angular, dismembered blocks of the host charnockite gneiss, suggesting localized brittle fragmentation superimposed on the ductile deformation fabric (Fig. 2c).

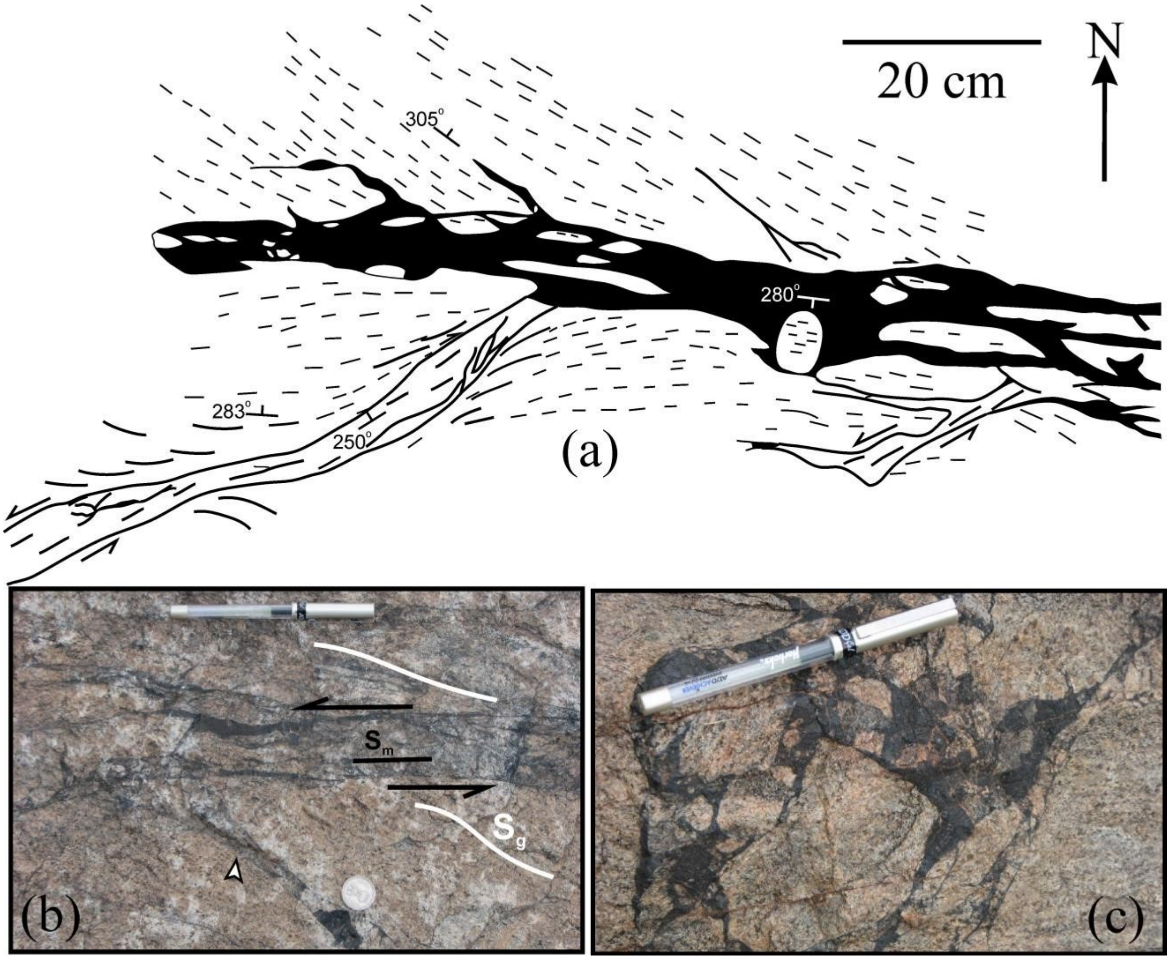

Fig. 2. Outcrop scale map of charnockite-hosted pseudotachylite veins (thick dark bands). Wider veins are parallel to the shear foliation (dextral sense of shear). The thinner pseudotachylite veins occur along C′ and C′′ shear bands, and the gneissic fabric (dotted lines) curves into the C-fabric. (b) Field photo showing wider pseudotachylite veins parallel to the shear zone foliation, S_m (parallel to pen; 14 cm long), and thinner veins (indicated by white arrow head) emplaced along the curved early gneissic layering (S_g). (c) Pseudotachylite forming vein networks with dismembered angular blocks of host charnockite gneiss. Pen length is 14 cm.

The Sellnaicekenpally segment of the Salem–Attur Shear Zone provides an ideal natural laboratory to investigate grain-size reduction associated with pseudotachylite formation in the lower crust. The close association of pseudotachylite veins with mylonitic fabrics enables evaluation of the roles of frictional melting, mechanical comminution, and subsequent recrystallization in grain-size evolution. These microstructural changes are critical for understanding strain localization, rheological weakening, and the long-term evolution of deep crustal shear zones (Biswal et al., 2010).

3. Grain size analysis: methodology

Size analyses were conducted on clasts within three pseudotachylite veins (couple-of-centimeters to sub-centimeter wide) hosted in charnockites (Fig. 3a, b). The thin and discontinuous pseudotachylite veins occurring over expansive charnockite outcrops (area of several thousand square meters) imply in situ formation. Veins too thin to yield robust statistics were excluded. In the host charnockite, quartz and plagioclase are the dominant minerals, with K-feldspar, hornblende, biotite, orthopyroxene and ilmenite present in lesser amounts; apatite and zircon are accessory. The shear-zone fabric is characterized by aggregates of fine-grained quartz and feldspars; these form linear trails that warp around larger polygonized grains and show internal strain in orthopyroxene (strain-induced wavy extinction, bent cleavage).

Size-frequency variations were estimated by first assembling high-resolution back-scattered electron

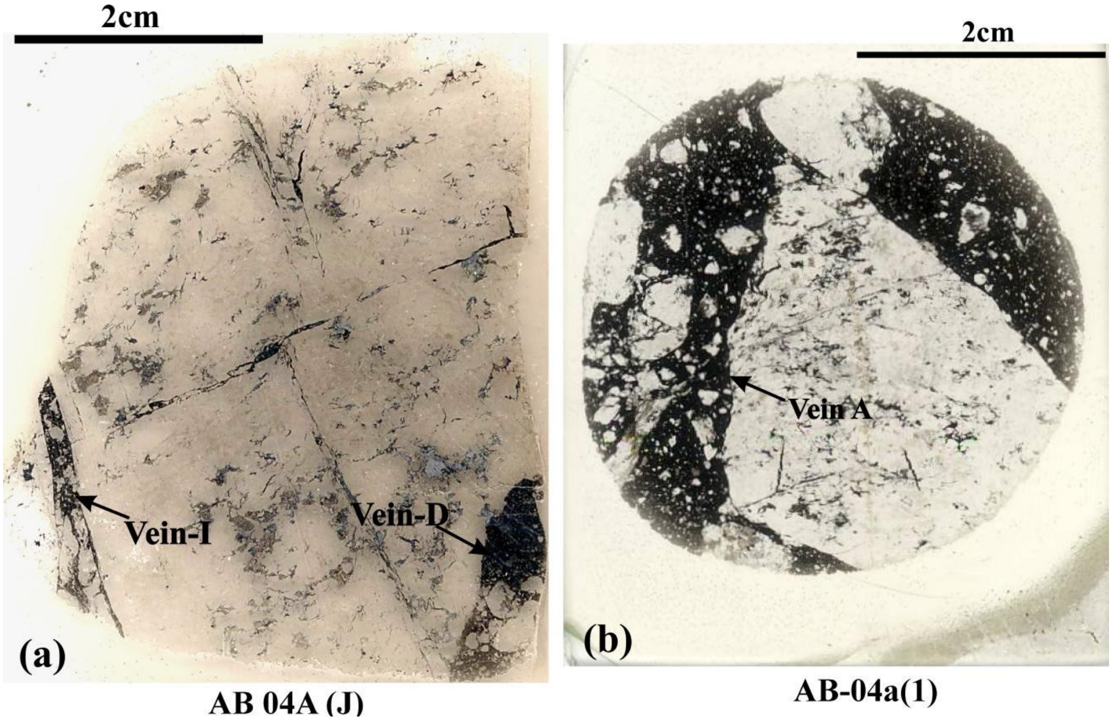

Fig. 3. Optically scanned images (a, b) of AB04A-J and AB04A-I showing pseudotachylite veins D, I and A in the sheared charnockite.

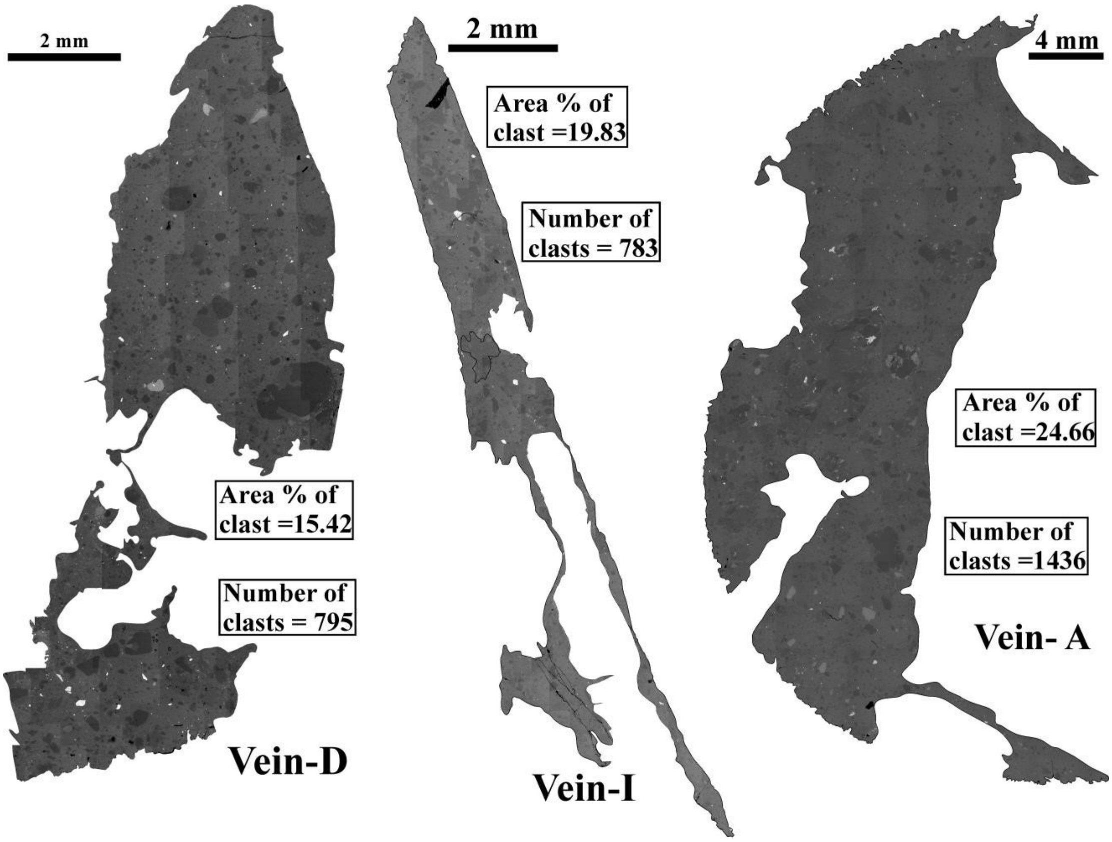

Fig. 4. BSE images of the three pseudotachylite veins D, I and A (occurrence shown in Fig. 3).

(BSE) images of the entire thin section into a single composite (Fig. 3). Margins of the pseudotachylite veins and clast boundaries were traced with precision (Fig. 4). The interior of each traced clast was filled

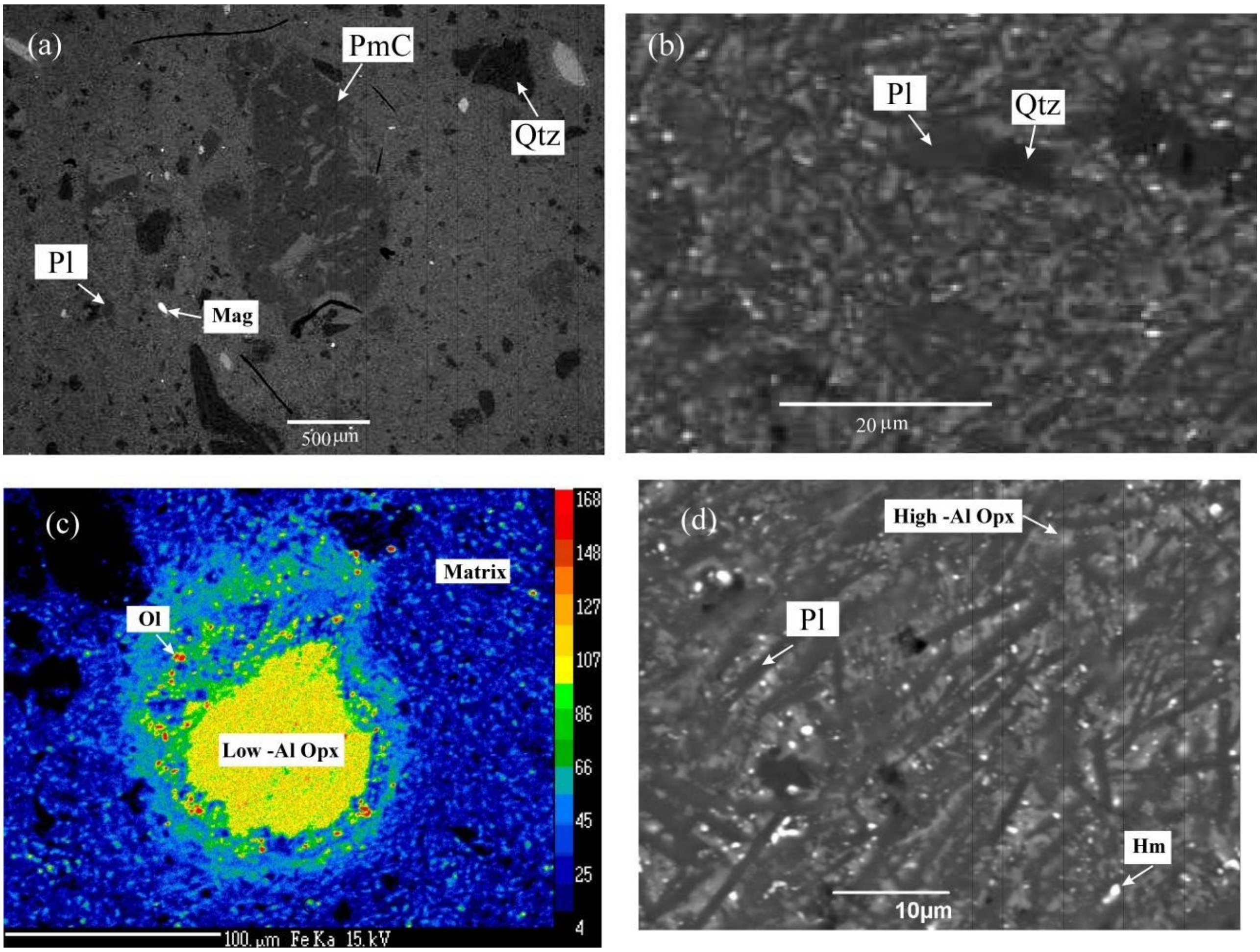

Fig. 5. Textures in pseudotachylites. (a) BSE image showing multiple types of clasts embedded in the matrix in vein-D. (b) BSE image showing fuzzy margins of clasts ∼ 10 µm in diameter. Also the clast interiors appear to contain minerals in the external fine-grained matrix. (c) X-ray element intensity maps of Fe showing reaction rims around clasts of low-Al orthopyroxene chemically similar to those in the host rock. Few bright red spots are hematite (absent in the host rock). (d) Inter-granular texture comprising euhedral plagioclase crystals (dark shade) and Fe, Al-rich Opx (lighter shade) filling up open spaces within plagioclase. Mineral abbreviations are after Kretz (1983). PmC is the acronym for poly-mineralic clast. Note occurrence of hematite.

with a color to ensure accurate representation of size and shape, after which the tracing line was removed. This approach minimizes mischaracterization of grain size and shape.

Across the three veins, only clasts with sharply defined, unambiguous margins were used, with maximum observed lengths of ∼20 µm. These clast sizes exceed the grinding limit for quartz (≈2 µm diameter; Steier and Schönert, 1972), but many quartz and feldspar clasts display fuzzy margins with the surrounding matrix, causing limited contrast in gray shade (Fig. 5a, b). This direct measurement method is preferred over image-processing approaches that rely on shade-enhanced BSE slicing, because it minimizes (i) shade-overlap effects at interfaces between unlike minerals and (ii) misidentification when matrix and clasts share similar grayscale values.

Clast mineralogy was determined by energy-dispersive spectroscopy (EDS) on a JEOL 6490 SEM, and major- and trace-element compositions were obtained for mono- and poly-mineralic clasts with a CAMECA SX-100 EPMA (Geology and Geophysics, IIT Kharagpur). Clasts comprise (i) mono-mineralic grains (predominantly quartz and plagioclase; smaller amounts of K-feldspar, ilmenite, and pyroxenes; accessory apatite and zircon) and (ii) poly-mineralic fragments of the host rock (Fig. 5a–b). The matrix contains microlites of fayalitic olivine and hematite, with patches of euhedral plagioclase microcrystals and Fe- and Al-rich orthopyroxene forming an inter-granular texture (Fig. 5d); such micro-crystals are absent in the host rock and may reflect rapid crystallization from melts or incongruent melting of host minerals (Patro et al., 2011).

Circular to elliptical quartz clasts with rounded margins are the dominant clast type in all three veins (Fig. 6), followed by plagioclase clasts. Poly-mineralic clasts are among the largest but are far less abundant than quartz and plagioclase clasts (Fig. 6). Clasts of K-feldspar, orthopyroxene, and ilmenite with strongly embayed margins are rare (Fig. 6); biotite and hornblende clasts are not observed. Given the very small counts of ilmenite and ferromagnesian phases, size-frequency analyses were not performed for these minerals individually; their contributions were incorporated into the pooled all-clast GSDs. Clast dimensions (area and radii) were measured from traced images with ImageJ (v1.38). Minimum and maximum radii (RA, RB) were obtained by ellipse-fitting, and the equivalent radius RE was calculated as RE = sqrt(RA × RB) (Simonato and Nagahama, 1992). The area outside the clasts (non-clast mosaic) in the three veins accounts for 75–85% of the total vein area (Fig. 4).

4. Results of grain size analyses

The largest clasts are invariably polymineralic and show substantial variation among the three veins. The maximum clast length corresponds to approximately 1.1 mm in vein A, 0.8 mm in vein D, and 0.4 mm in vein I (Figs. 4, 6). Generally, thinner veins host smaller maximum clasts (Figs. 4, 6). In the ensuing discussion, the equivalent radii of the largest clasts are taken as ∼915 µm (vein A), ∼450 µm (vein D), and ∼250 µm (vein I) (Fig. 7). The largest clasts in each vein were excluded for two reasons. First, the long-tail decline of low-abundance, coarser clasts compresses the size-frequency variations at finer sizes (Fig. 7). Consequently, including coarser grains reduces the apparent variation in the fine-size domain. Second, in the coarser size range, the clast counts are 1, 2, and 0 for the smallest bins, making those “zero” values unsuitable for log–log plotting. The measured clast counts are 794 (vein D), 782 (vein I), and 1,436 (vein A). After excluding the coarsest grains, the counts used for generating GSDs are 789 (99% of total) for vein D, 770 (98%) for vein I, and 1,420 (99%) for vein A.

Histograms and cumulative frequency plots at a 15 µm bin size, incorporating all clasts, are compared with those for quartz, feldspar, and polymineralic clasts (Fig. 7). For this size range, the following generalizations apply at 15 µm bin size: (a) clast sizes (mono-mineralic plus poly-mineralic) in each vein approximate a normal distribution, though the finer-size data are truncated by limited sampling; (b) size-frequency patterns for polymineralic clasts differ from those for quartz and plagioclase clasts; (c) the most abundant polymineralic clasts are coarser than the most abundant quartz clasts; (d) the modal size of all clasts pooled together matches the modal size of quartz and plagioclase across the three veins; (e) mono- and polymineralic clasts show decreasing abundance away from the peak, broadly following a Gaussian-like distribution; (f) in the coarser size range, the all-clasts pool exhibits non-smooth declines, punctuated by spiking due to high-abundance, low-frequency polymineralic and monomineralic grains other than quartz (feldspar in vein I).

The log(Nn) versus log(rn) relationships for all clasts pooled together become more linear with increasing bin size (Fig. 8). At the smallest bin size (15 µm), the curves are curved because finer grains fall off the trend defined by coarser grains, yielding poor linear fits with D values < 1.5 (Fig. 8). With larger bin sizes, the fine-grain fall-off diminishes and linearity improves. At a 50 µm bin size, reasonably good linear fits ($R2 \geq 0.92$) are obtained, with D values between 2 and 3. Similar bin-size–dependent behavior is observed for the quartz clasts of lower abundance (Data Repository2).

5. Discussion

All clasts taken together, poly-mineralic clasts and mono-mineralic clasts independently exhibit ill-defined Gaussian GSDs at smaller bin sizes. At larger bin sizes, the abundances of the finer grains are “grouped” with the high abundance peak, and this leads to manifold increase in the overall abundance of the finer size fraction, but at the other end of the size spectrum, i.e. in the coarser size fraction, fewer grains are “pooled in” and thus the cumulative abundance of the coarse grains increase marginally with increasing bin size. The combined effect is to increase in the abundance of clasts in the different bins (relative to smaller bin sizes) as well as steepening of the slope (higher D values) of the log (N_n) versus log (r_n) plots at the higher bin sizes. In the clasts size range (15–950 µm) investigated, by expanding or stretching the bin size to 30 µm and 50 µm, the GSD patterns in the clasts changed from seemingly

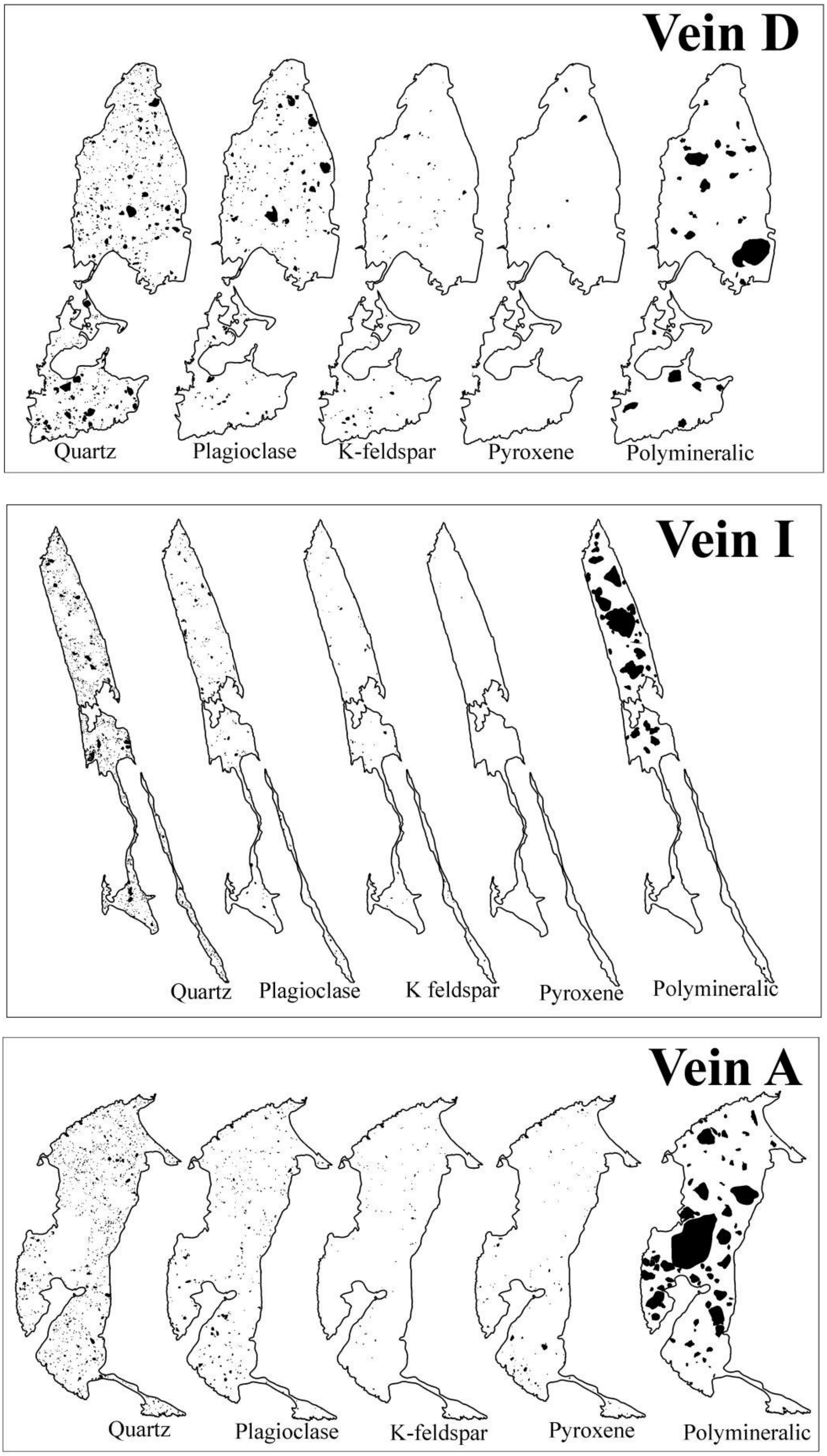

Fig. 6. The distribution of different types of clasts in the three veins, e.g. (a) vein-D, (b) vein-I and (c) vein-A. Clasts of apatite and zircon are not shown.

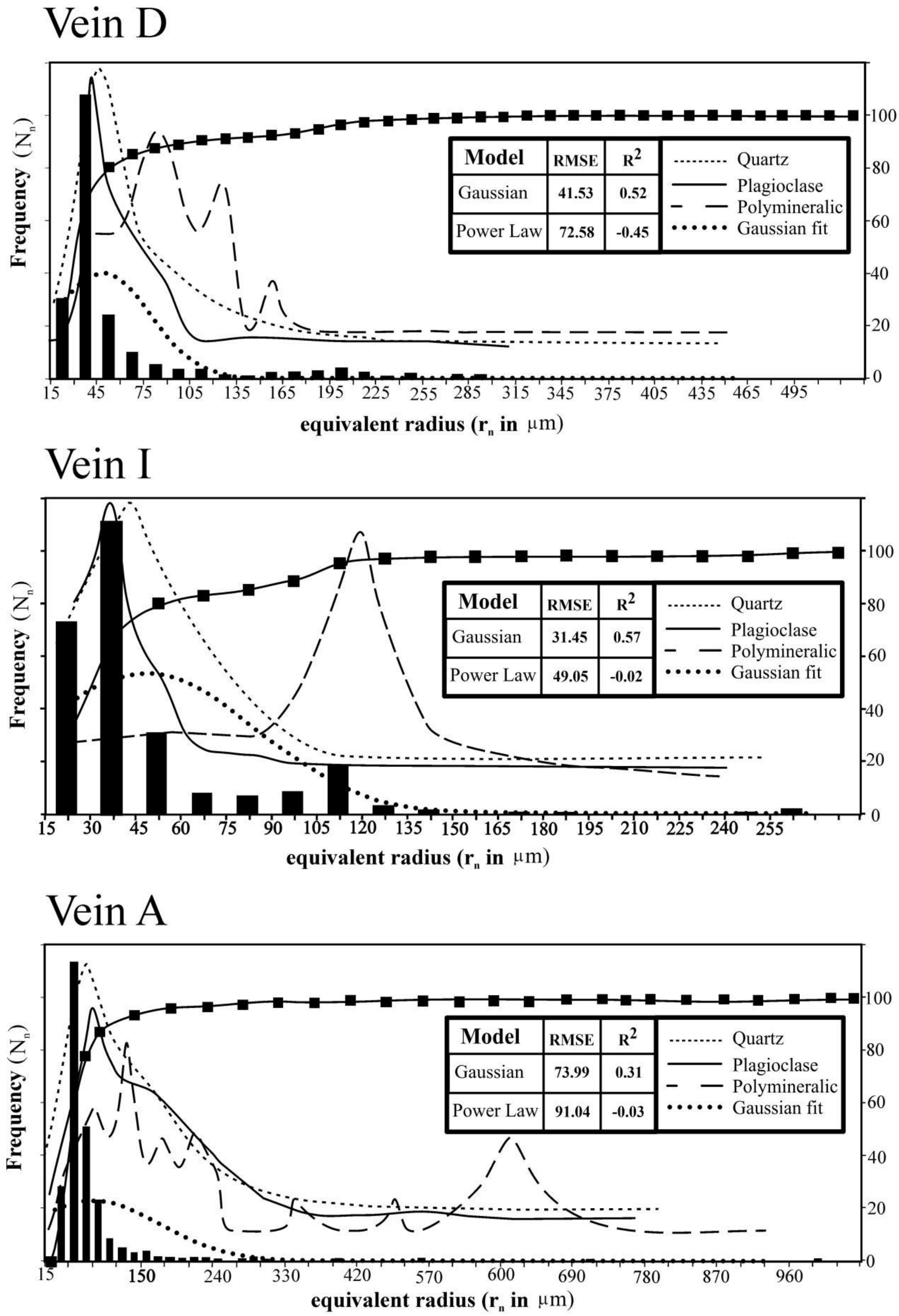

Fig. 7. Histograms (filled bar) and cumulative frequency (filled square) plots of all clasts taken together in each of the three veins (bin size is 15 µm). The numbers keyed to the left and right vertical axes refer to the bar diagrams and the frequency plots respectively. The vertical axis in the right (for cumulative percentage) is scaled from 0 to 100, but the vertical axis to the left (for histogram) is not scaled. The frequency distribution of quartz (dashed line) and plagioclase (continuous line) clasts, clasts of poly-mineralic aggregates (broken line) and Gaussian fit (dotted line) in the veins are shown (the actual bar diagrams and the cumulative frequency plots for quartz and plagioclase clasts and the poly-mineralic clasts are presented in the Data Repository)[1]. Note lines for mono-mineralic and poly-mineralic clasts are drawn by joining (without smoothening) the frequency of clasts at the median size value in each bin size.

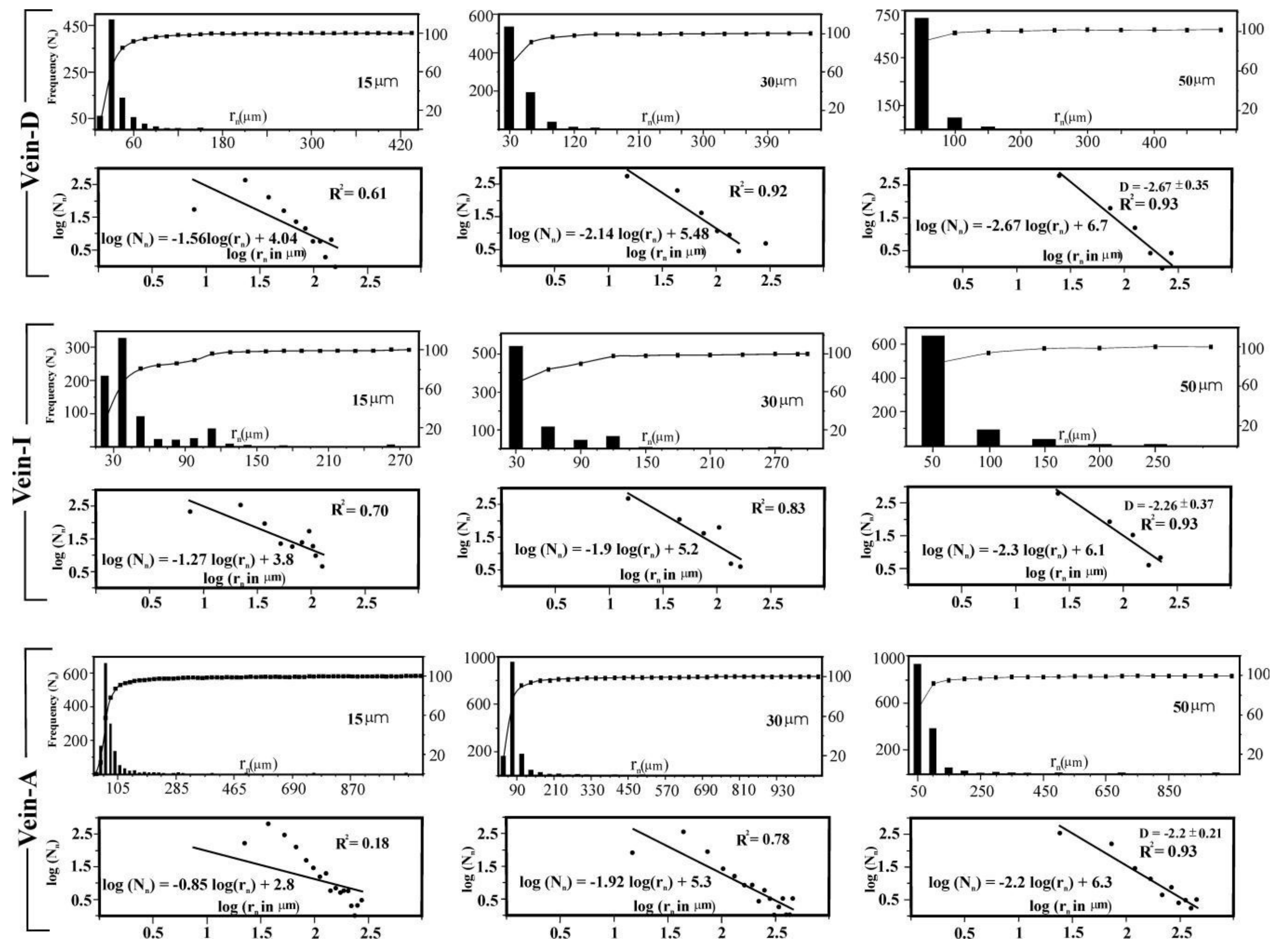

Fig. 8. Bar diagram and cumulative frequency plots (top-set) and the corresponding log (r_n) vs. log (N_n) plots (bottom set) are shown for all clasts pooled together in the three veins are compared for bin sizes 15, 30 to 50 µm. Bottom set images in each of the paired images show straight line fit to log (r_n) vs. log (N_n) plots (filled circles). R^2 and the regression equations to the straight line fits are indicated. 2σ errors for D values are shown for the highest R^2 values (>0.9) at 50µm bin size.

Gaussian distribution to power law distribution, i.e. the grain abundance monotonically increases with decreasing grain size (Fig. 8), manifested by linear fit to negatively-correlated GSD in log (N_n) versus log(r_n) plots with R^2 values at 0.93 at 50 µm bin size. If the power law distribution at high bin sizes is assumed to be fractal in nature, the abundances of the finer sizes in the investigated size range are predicted to be more abundant than the most abundant size (Fig. 8) in contradiction to the measured values. The size-frequency data for mono-mineralic and poly-mineralic clasts in each vein (Data Repository[1]) show similar modifications with increasing bin size. It follows that the power law approximation and the resultant D value are not valid outside the stated range. In other words, the power law approximation of GSDs in the pseudotachylite examined is non-fractal in nature, and does not suggest that the abundances of finer grains beyond the size range investigated monotonically increase.

This interpretation is further supported by the histogram-based goodness-of-fit statistics, which evaluate how accurately the different models reproduce the observed grain-size frequency distributions. Across all three datasets, the Gaussian model consistently yielded lower RMSE (Root Mean Square Error) values and higher R^2 (Coefficient of Determination) values than the power-law model, indicating a closer agreement with the observed grain-size distributions. These results further support the interpretation that the apparent power-law behaviour observed at larger bin sizes is primarily an artefact of bin-size selection rather than evidence of a true fractal grain-size distribution. Therefore, the Gaussian model provides a more appropriate representation of the overall grain-size distributions of the investigated pseudotachylite clasts.

Alternative explanations for the observed grain-size distributions were also considered. Post-formational alteration, recrystallisation, or grain growth could potentially modify the primary grain-size distribution, while sampling bias arising from sectioning effects or limitations in identifying the smallest grains may contribute to the truncation of the finer grain-size fraction. However, the Salem pseudotachylites preserve sharp vein boundaries, flow textures, and well-developed orthopyroxene and plagioclase micro-phenocrysts, with no evidence of pervasive recrystallisation or alteration that could significantly modify the primary clast population. Furthermore, the consistency of the grain-size distributions across all three veins suggests that the observed trends are robust and are unlikely to be artefacts of sampling or analytical limitations. Therefore, although these factors cannot be completely ruled out, they are unlikely to account for the observed non-fractal grain-size distributions or the predominance of the fine-grained matrix.

Also, the abundance patterns of the polymineralic aggregates, and monomineralic quartz and plagioclase clasts are not identical. This implies that the processes of comminution of poly-mineralic aggregates (≈ host rock fragment) and mono-mineralic grains were different, presumably determined by the rheological properties of the different materials (Spray, 2010) and the actual processes of grain comminution, e.g. by rupture, wear or attrition (Keulen et al., 2007). Clasts measured with the naked eye and measured in outcrops (ignored in this study) are typically larger than individual minerals in the host rock and are likely to be populated with coarser poly-mineralic aggregates (Figs. 2a, 3) in contrast to the majority of smaller clasts measured under the optical/scanning electron microscope dominated by mono-mineralic clasts, quartz and feldspars being common (cf. Fig. 6). Since the rheology of mono-mineralic and poly-mineralic clasts influences grain comminution, log (r_n) vs. log (N_n) plot of GSD data pooled from mesoscopic and microscopic sized clasts in the same outcrop is unlikely to yield straight line fits with unique D values due to subtle variations in the clast mineralogy and comminution processes thereof (cf. Keulen et al., 2007). Thus curvatures and inflections in the log (r_n) vs. log (N_n) plots (non-unique D values) are manifestations of rheology accommodated grain comminution processes (Keulen et al., 2007; Spray, 2010). Thus, log-linear plot of r_n versus N_n in the stated size ranges for specific bin sizes is fractal for rheologically similar minerals.

5.1. The nature of the fine-grained matrix

For Gaussian distribution of grain sizes, the area of the clasts smaller in size than those at the frequency peak is manifold smaller than the area occupied by the clasts larger than the frequency peak. Since all clasts together in the range investigated comprise 20–25% of the total area of the veins, it stands to reason that the combined area of the fraction of the smaller clasts beyond the size range investigated can only constitute a few percent of the non-clast matrix area, i.e. 75–85% of the total area of the veins (Shimamoto and Nagahama, 1992). We suggest therefore that the fine-grained matrix in all probability was composed of quenched melts studded with micro-phenocrysts precipitated from friction-induced melt. The melt origin for the fine-grained matrix is supported by the presence of flow textures in Opx microphenocrysts (Fig. 5c) and inter-granular intergrowths among idiomorphic micro-crystals of orthopyroxene and plagioclase (Fig. 5d).

5.2. The “fall-off in the finer-size range

The origin of the “fall-off” in the finer-size range (Shimamoto and Nagahama, 1992; Ray, 1999; Keulen et al., 2007; this study) requires consideration of both analytical limitations and geological processes. Although incomplete detection of the smallest grains may contribute to the truncation of the grain-size distribution, the systematic nature of the fall-off observed in all three veins indicates that it primarily reflects natural processes. On melting, the comminuted clasts experience reduction in size (equivalent radius), and therefore the pre-melting GSD is modified towards smaller sizes (Fig. 9a–c). The effect of melting on size frequency is more complex. If the number of grains “hopping in” from coarser sizes to a particular smaller size (due to size reduction on melting) is less than the number of grains “hopping out” from the particular size (due to melting), the frequency of the particular size will decrease (Fig. 9a). For the converse, the frequency will increase (Fig. 9b), but the frequency will remain unchanged if the grains “hopping in” and “hopping out” are equal (no change in frequency with decreasing size). But due to melting,

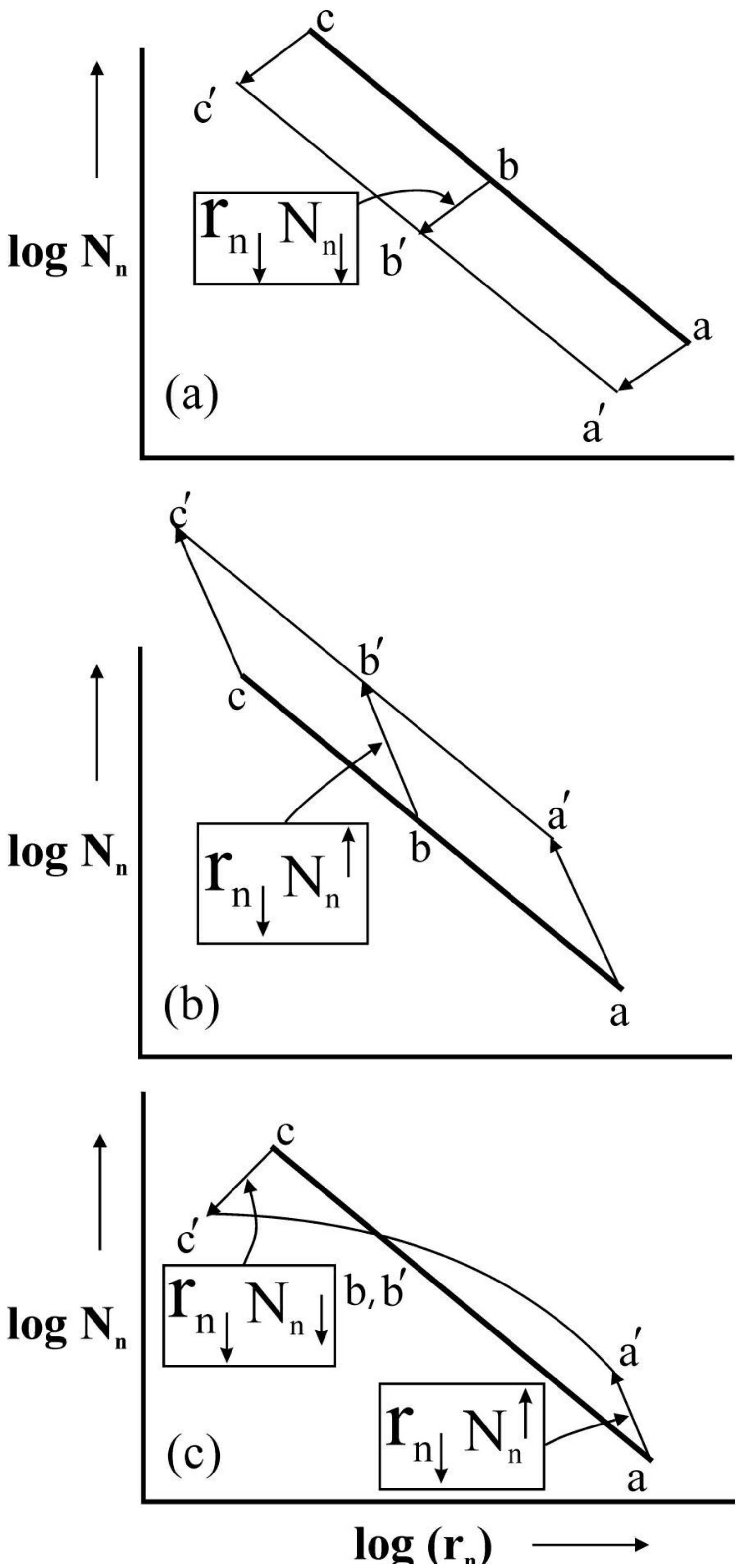

Fig. 9. (a–c): Assuming power law grain-size distribution in pseudotachylites, sketches show possible ways along which size of comminuted grains may change due to melting (bold continuous line for pre-melting GSD; and thin, continuous line for post-melting GSD). r_n is the equivalent radius on n grains; N_n is the frequency of n grains. Short arrows show direction of change. a, b and c are points of the pre-melting GSD plot, and a′, b′ and c′ are the corresponding points in the post-melting GSD. (a) Grains "hopping in" are less than grains "hopping out" (decrease in N_n). (b) Grains "hopping in" are more than grains "hopping out" (increase in N_n). (c) Finer grains (for r_n values < b) are being preferentially consumed (by melting) more than the grains hopping in (N_n decreases); for grains with r_n values > b, N_n increases, in the absence of grain consumption by melting.

a fraction of the smallest grains may be consumed or size reduction on melting may make these clasts too small to be identified. This will cause the frequency of the smallest grains to decrease, and will result in the "fall-off" in the finer size range if the decrease in the abundance is more relative to the coarser sizes (Fig. 9c).

The resulting convex upward shape of the N_n vs r_n grain size variation (Fig. 9c) is therefore the consequence of grain size comminution by the combined effects of grain attrition by friction and friction-induced melting. Since friction-induced grain attrition is likely to be minimal or ineffective in partially molten rocks because grain-grain contacts are either lost or lubricated, the "fall-off" of the finer grains from the linear plot may be best explained if friction-induced attrition is followed by melting or both processes occur in tandem, albeit at low melt fraction.

6. Conclusions

We document from size-frequency analyses of clasts in Salem pseudotachylites that the GSDs of the clasts are non-fractal, and cannot be described by power law approximation unless the bin sizes are enhanced to larger sizes. By suitably expanding or stretching the bin size (class intervals) the grain size variations can be approximated to power law distribution for the size range investigated. The approximation is validated for higher bin sizes because of the manifold increase in the abundances of the finer size fraction (relative to the coarser size fraction) due to the grouping of the abundances of the finer sizes with the peak abundance. In other words, the power law approximation does not have genetic implications beyond the size range investigated. The GSDs of mono-mineralic and polymineralic clasts are different possibly reflecting non-uniform grain size comminution is influenced by the rheology of the materials being crushed and the grain-size reduction processes. We argue that the non-clast area fraction of the fine-grained matrix cannot be satisfactorily explained by the finer-sized aggregates beyond the size range investigated, and therefore the bulk of the dark ultra-fine grained matrix is composed of quenched melts and micro-phenocrysts that crystallized from the melts prior to quenching.

AI-statement

No AI tool was used to generate process, analyze, or interpret scientific data or for scientific interpretations, or formulate the results and conclusions in the manuscript. The research, analysis, interpretation, and scientific conclusions were carried out entirely by the authors based on the data and observations obtained from the study.

CRediT statement

HD: Conceptualization, Methodology, Investigation, and Writing—Original Draft. AB: Methodology, Visualization, and Writing—Review & Editing. AG: Figure Preparation and Reference Management, Writing. NPU: Figure Preparation and Calculations.

Acknowledgments

The authors acknowledge that this research was carried out by the first author as part of the SMNRI project at Cochin University. The authors are grateful to the National EPMA Facility, Department of Geology and Geophysics, IIT Kharagpur, for providing Electron Probe Microanalysis (EPMA) facilities and analytical support.

Appendix A.

Bar diagrams and cumulative frequency plots for quartz, plagioclase and poly-mineralic clasts in each of the three veins at bin sizes 15, 30 to 50 μm.

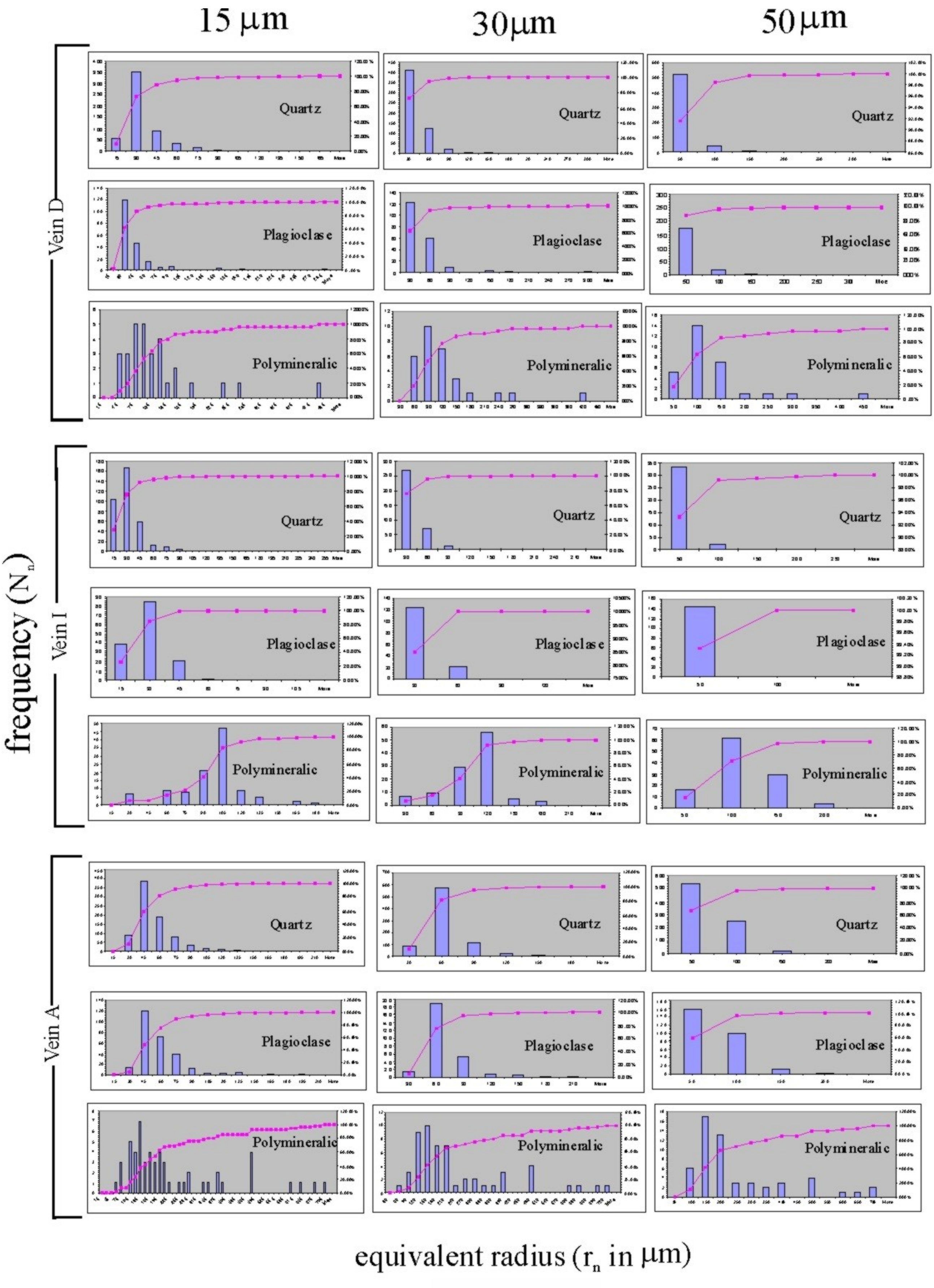

15 μm
30μm
50μm
Vein D
Vein I
Vein A
Quartz
Plagioclase
Polymineralic
frequency (Nn)
equivalent radius (rn in μm)

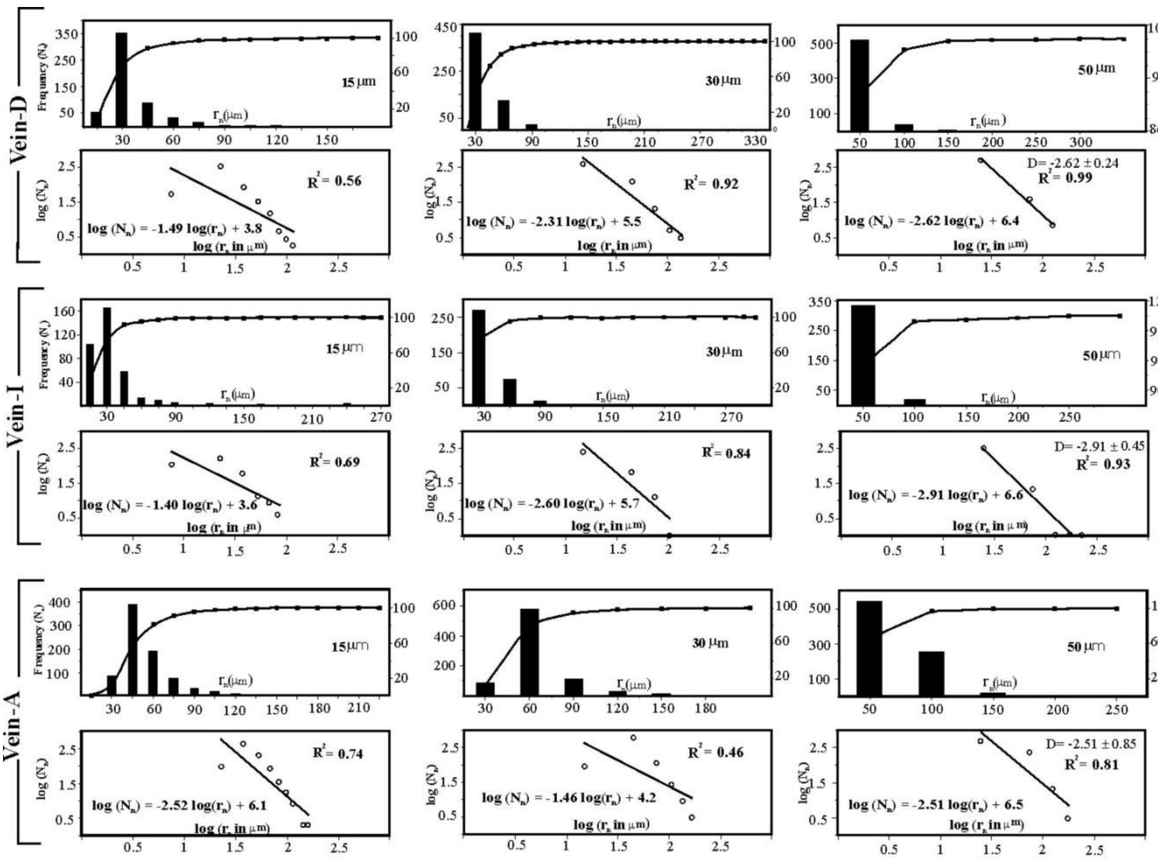

Appendix B.

Bar diagrams and cumulative frequency plots (top-set images) and log (r_n) vs. log (N_n) plots (bottom set images) for quartz clasts in each of the three veins are compared for bin sizes 15, 30 to 50 µm. Bottom set images in each of the paired images show straight line fit to log (r_n) vs. log (N_n) plots (filled circles). R^2 and the regression equations to the straight line fits are indicated. 2σ errors for D values are shown for the highest R^2 values (>0.9) at 50µm bin size.

References

Bhadra, B.K., 2001. Ductile shearing in Attur shear zone and its relation with Moyar shear zone, south India. *Gondwana Research* 3, 361–370. https://doi.org/10.1016/S1342-937X(05)70294-X.

Bhadra, S., Das, S., Bhattacharya, A., 2007. Shear zone-hosted migmatites (Eastern India): The role of dynamic melting in the generation of REE depleted felsic melts, and implications for disequilibrium melting. *J. Petrol* 48, 435–457. https://doi.org/10.1093/petrology/egl066.

Bhaskar Rao, Y.J., Chetty, T.R.K., Janardhan, A.S., Gopalan, K., 1996. Sm-Nd and Rb-Sr ages and P-T history of the Archaean Sittampundi and Bhavani layered complexes in the Cauvery shear zone, South India: evidence for Neoproterozoic reworking of Archaean crust. *Contri. Miner. Petrol* 125, 237–250. https://doi.org/10.1007/s004100050219.

Bhaskar Rao, Y.J., Janardhan, A.S., Vijaya Kumar, T., Narayana, B.L., Dayal, A.M., Taylor, P.N., Chetty, T.R.K., 2003. Sm–Nd Model Ages and Rb–Sr isotopic systematics of charnockites and gneisses across the Cauvery Shear Zone, Southern India: implications for the Archaean–Neoproterozoic terrane boundary in the Southern Granulite Terrain, in: Ramakrishnan, M. (Ed.), *Tectonics of Southern Granulite Terrain — Kuppam–Palani Geotransect. Geol. Soc. India Memoir.* volume 50, p. 297–317.

Biswal, T.K., Thirukumaran, V., Kamleshwar, R., Bandyapadhya, K., Sundaralingam, K., Mondal, A.K., 2010. A study of mylonites from parts of the Salem-Attur shear zone (Tamil Nadu) and its tectonic implications. *Journal of Geological Society of India* 75, 128–136. https://doi.org/10.1007/s12594-010-0002-3.

Blanpied, M., Lockner, D., Byerlee, J., 1995. Frictional slip of granite at hydrothermal conditions. *Journal of Geophysical Research* 100, 13045–13064. https://doi.org/10.1029/95JB00862.

Blenkinsop, T.G., Sibson, R.H., 1992. Aseismic fracturing and cataclasis involving reaction softening within core material from the Cajon Pass Drill Hole. *Journal of Geophysical Research* 97(B4), 5135–5144. https://doi.org/10.1029/90JB02285.

Brandt, S., Schenk, V., Raith, M.M., Appel, P., Gerdes, A., Srikantappa, C., 2011. Late Neoproterozoic P-T evolution of HP-UHT granulites from the Palni Hills (south India): New constraints from phase diagram modeling, LA-ICP-MS zircon dating and in-situ EMP monazite dating. *Journal of Petrology* 52, 1813–1856. https://doi.org/10.1093/petrology/egr032.

Brown, M., Solar, G.S., 1998. Granite ascent and emplacement during contractional deformation in convergent orogens. *Journal of Structural Geology* 20, 1365–1393. https://doi.org/10.1016/S0191-8141(98)00074-1.

Caricchi, L., Burlini, L., Ulmer, P., Gerya, T., Vassali, M., Papale, P., 2007. Non-Newtonian rheology of crystal-bearing magma and implications for magma ascent dynamics. *Earth and Planetary Science Letters* v. 264, 402–419. https://doi.org/10.1016/j.epsl.2007.09.032.

Champallier, R., Bystricky, M., Arbaret, L., 2008. Experimental investigation of magma rheology at 300 MPa: from pure hydrous melt to 76 vol.% crystals. *Earth and Planetary Science Letters* v.267, 571–583. https://doi.org/10.1016/j.epsl.2007.11.065.

Chester, J., Chester, F., Kronenberg, A., 2005. Fracture surface energy of the Punchbowl fault. *San Andreas system. Nature* 437, 133–136. https://doi.org/10.1038/nature03942.

Chetty, T.R.K., 1996. Proterozoic shear zones in Southern Granulite Terrain, in: Santosh, M., Yoshida, M. (Eds.), *The Archaean and Proterozoic Terrains in Southern India within East Gondwana India. Gondwana Research Group Memoir*. volume 3, p. 77–89.

Clarke, G.L., Norman, A.R., 2007. Generation of pseudotachylite under granulite facies conditions, and its preservation during cooling. *Journal of Metamorphic Geology* 11, 319–335. https://doi.org/10.1111/j.1525-1314.1993.tb00151.x.

Davidage, R.W., 1979. *Mechanical Behavior of Ceramics*. Cambridge Univ. Press, Cambridge, UK.

Drury, S.A., Harris, N.B.W., Holt, R.W., Reeves-Smith, G.J., Wightman, R.T., 1984. Precambrian tectonics and crustal evolution in southern India. *Journal of Geology* 92, 3–20. https://doi.org/10.1086/628831.

Drury, S.A., Holt, R.W., 1980. The tectonic framework of the south Indian craton: a reconnaissance involving LANDSAT imagery. *Tectonophysics* 65, 1– 5. https://doi.org/10.1016/0040-1951(80)90073-6.

Gibson, R.L., 2002. Impact-induced melting of Archean granulites in the Vredefort Dome, South Africa. I: anatexis of metapelite granulite. *Journal of Metamorphic Geology* 20, 57–70. https://doi.org/10.1046/j.0263-4929.2001.00358.x.

Han, R., Shimamoto, T., Hirose, T., Ree, J..H., ando, J..I., 2007. Ultra low friction of carbonate faults caused by thermal decomposition. *Science* 316, 878–881. https://doi.org/10.1126/science.1139763.

Hand, M., Dirks, P.H.G.M., 1992. The influence of deformation on the formation of axial planar leucosomes and the segregation of small melt bodies within the migmatitic Napperby Gneiss, central Australia. *Journal of Structural Geology* 14, 591–604. https://doi.org/10.1016/0191-8141(92)90159-T.

Hirose, T., Shimamoto, T., 2005. Growth of molten zone as a mechanism of slip weakening of simulated faults in gabbro during frictional melting. *Journal of Geophysical Research* https://doi.org/10.1029/2004JB003207.

Jain, A.K., Singh, S., Manickavasagam, R.M., 2003. Intracontinental shear zones in the southern granulite terrain: their kinematics and evolution, in: Ramakrishnan (Ed.), *Tectonics of Southern Granulite Terrain, Kuppam-Palani Geotransect. Geological Society of India Memoir 50*, p. 225–253.

Janssen, C., Wirth, R., Rybacki, E., Naumann, R., Kemnitz, H., Wenk, H.R., Dresen, G., 2010. Amorphous material in SAFOD core samples (San Andreas Fault): evidence for crush-origin pseudotachylytes? *Geophysical Research Letters* 37, 01303,. https://doi.org/10.1029/2009GL040993.

Keulen, N., Heilbronner, R., Stunitz, H., Boullier, A..M., Ito, H., 2007. Grain size distributions of fault rocks: A comparison between experimentally and naturally deformed granitoids. *Journal of Structural Geology* 29, 1282–1300. https://doi.org/10.1016/j.jsg.2007.04.003.

Kretz, R., 1983. Symbols for rock-forming minerals. *American Mineralogist* 68, 277–279.

Lieger, D., Riller, U., Gibson, R.L., 2009. Generation of fragment-rich pseudotachylite bodies during central uplift formation in the Vredefort impact structure, South Africa. *Earth and Planetary Science Letters* 279, 53–64. https://doi.org/10.1016/j.epsl.2008.12.031.

Lund, M.G., Austrheim, H., 2003. High-pressure metamorphism and deep-crustal seismicity: evidence from contemporaneous formation of pseudotachylites and eclogite facies coronas. *Tectonophysics* 372, 59–83. https://doi.org/10.1016/S0040-1951(03)00232-4.

Macaudiere, J., Brown, W.L., Ohnenstetter, D., 1985. Microcrystalline textures resulting from rapid crystallization in a pseudotachylite melt in a meta-anorthosite. *Contributions to Mineralogy and Petrology* 89, 39–51. https://doi.org/10.1007/BF01177589.

Mandelbrot, B., 1982. *The fractal geometry of nature*. Freeman and Co, New York.

Meißer, B., Deters, P., Srikantappa, C., Köhler, H., 2002. Geochronological evolution of the Moyar, Bhavani and Palghat shear zones of southern India: implications for east Gondwana correlations. *Precambrian Research* 114, 149–175. https://doi.org/10.1016/S0301-9268(01)00222-4.

Mogi, K., 1974. On the pressure dependence of strength of rocks and the Coulomb-fracture criterion. *Tectonophysics* 21, 273–85. https://doi.org/10.1016/0040-1951(74)90055-9.

Obata, M., Karato, S., 1995. Ultramafic pseudotachylite from the Balmuccia peridotite, Ivrea-Verbano zone, northern Italy. *Tectonophysics* 242, 313–328. https://doi.org/10.1016/0040-1951(94)00228-2.

Okamoto, Y., Kitamura, M., 1990. A mineralogical study of pseudotachylites from Scotland, in: Abstract Annual Meeting of the Mineralogical Society of Japan.

Patro, R., Mahapatro, S.N., Bhattacharya, A., Pant, N.C., Nanda, J.K., Dey, A., Tripathy, A.K., 2011. Chemical heterogeneity in an enderbite-hosted pseudotachylite, eastern India: evidence for syn-deformation multi-reaction melting in pseudotachylite. *Contributions to Mineralogy and Petrology* 161, 547–563. https://doi.org/10.1007/s00410-010-0548-5.

Pec, M., Stunitz, H., Heilbronner, R., Drury, M.de.Capitani, C., 2012. Origin of pseudotachylites in slow creep experiments. *Earth and Planetary Science Letters* 355–356, 299–310. https://doi.org/10.1016/j.epsl.2012.09.004.

Petford, N., Kerr, R.C., Lister, J.R., 1993. Dile transport of granitoid magmas. *Geology* v. 21, 845–848. https://doi.org/10.1130/0091-7613(1993)021.

Plattner, U., Markl, G., Sherlock, S., 2003. Chemical heterogeneities of Caledonian (?) pseudotachylites in the Eidsfjord Anorthosite, north Norway. *Contributions to Mineralogy and Petrology* 145, 316–338. https://doi.org/10.1007/s00410-003-0455-0.

Raisanen, M., Mertamo, M., Stenlid, L., Viitanen, J., 2006. Laboratory crushing of rock aggregates. Paper No. IAEG2006 Paper number 411;.

Raith, M., Srikantappa, C., Buhl, D., Koehler, H., 1999. Nilgiri enderbites, South India: nature and age constraints on protolith formation, high-grade metamorphism and cooling history. *Precambrian Research* 98, 129–150. https://doi.org/10.1016/S0301-9268(99)00045-5.

Ramakrishnan, M., 2003. Craton-mobile belt relations in Southern Granulite Terrain, in: Ramakrishnan (Ed.), *Tectonics of Southern Granulite Terrain, Kuppam-Palani Geotransect. Geological Society of India Memoir.* volume 50, p. 1–24.

Ray, S.K., 1999. Transformation of cataclastically deformed rocks to pseudotachylite by pervasion of frictional melt: inferences from clast-size analysis. *Tectonophysics* 301, 283–304. https://doi.org/10.1016/S0040-1951(98)00229-7.

Rosenberg, C.L., 2001. Deformation of partially-molten granite: a review and comparison of experimental and field investigations. *The International Journal of Earth Sciences* 90, 60–76. https://doi.org/10.1007/s005310000164.

Sammis, C., King, G., Biegel, R., 1987. The kinematics of gouge deformation. *Pure and Applied Geophysics* 125, 777–812. https://doi.org/10.1007/BF00878033.

Satheesh Kumar, R., Prasannakumar, V., 2009. Fabric evolution in Salem-Attur Shear Zone, South India, and its implications on the kinematics. *Gondwana Research* 16, 37–44. https://doi.org/10.1016/j.gr.2008.10.006.

Shand, S.J., 1916. The pseudotachylite of Parijs (Orange Free State) and its relation to :trap-shotten gneiss” and “flinty crush-rock”. *Quarterly Journal of the Geological Society of London* 72, 198–221. https://doi.org/10.1144/GSL.JGS.1916.072.01-04.12.

Shimamoto, T., Nagahama, H., 1992. An argument against the crush origin of pseudotcahylytes based on the analysis of clast-size distribution. *Journal of Structural Geology* 89, 999–1006. https://doi.org/10.1016/0191-8141(92)90031-Q.

Skrotzki, W., A., Wedel., Weber, K., Müller, W.F., 1990. Micro-structure and texture in Iherzolites of the Balmuccia massif and their significance regarding the thermomechanical history. *Tectonophysics* 179, 227–251. https://doi.org/10.1016/0040-1951(90)90292-G.

Spray, J.G., 2010. Frictional Melting Processes in Planetary Materials: from hypervelocity impact to earthquakes. *Annual Reviews in Earth and Planetary Sciences* 38, 221–54. https://doi.org/10.1146/annurev.earth.031208.100045.

Steier, K., Schönert, K., 1972. Verformung und Bruchpha ̈nomene unter Druckbeanspruchung von sehr kleinen Ko ̈rnern aus Kalkstein, Quarz und Polystyrol. *Dechema Monograph* 69, 167–192.

Toyoshima, T., 1989. Pseudotachylite from the main zone of the Hidaka metamorphic belt, Hokkaido, Northern Japan. *Journal of Metamorphic Geology* 8, 507–523. https://doi.org/10.1111/j.1525-1314.1990.tb00483.x.

Tromans, D., Meech, J.A., 2002. Fracture toughness and surface energies of minerals: theoretical estimates for oxides, sulphides, silicates and halides. *Mineral Engineering* 15, 1027–41. https://doi.org/10.1016/S0892-6875(02)00213-3.

Turcotte, D.L., 1992. *Fractals and Chaos in Geology and Geophysics.* Cambridge Univ. Press, Cambridge, UK.

Vigneresse, J.L., Barbey, P., Cuney, M., 1996. Rheological transitions during partial melting and crystallization with application to felsic magma segregation and transfer. *Journal of Petrology* 37, 1579–1600. https://doi.org/10.1093/petrology/37.6.1579.

Wenk, H..R., 1978. Are pseudotachylites products of fracture or fusion? *Geology* 6, 507–511. https://doi.org/10.1130/0091-7613(1978)6.

Wenk, H..R., Johnson, L.R., Ratschbacher, L., 2000. Pseudotachylites in the eastern Peninsular ranges of California. *Tectonophysics* 321, 253–277. https://doi.org/10.1130/0091-7613(1978)6.

Wilson, B., Dewers, T., Reches, Z., Brune, J., 2005. Particle size and energetics of gouge from earthquake rupture zones. *Nature* 434, 749–752. https://doi.org/10.1038/nature03433.

